

Large-scale multilayer architecture of single-atom arrays with individual addressability

Malte Schlosser,* Sascha Tichelmann, Dominik Schäffner, Daniel Ohl de Mello, Moritz Hambach, and Gerhard Birkl†
*Institut für Angewandte Physik, Technische Universität Darmstadt,
 Schlossgartenstraße 7, 64289 Darmstadt, Germany*
 (Dated: May 22, 2019)

We report on the realization of large-scale 3D multilayer configurations of planar arrays of individual neutral atoms with immediate applications in quantum science and technology: a microlens-generated Talbot optical lattice. In this novel platform, the single-beam illumination of a microlens array constitutes a structurally robust and wavelength-universal method for the realization of 3D atom arrays with favourable scaling properties due to the inherent self-imaging of the focal structure. Thus, 3D scaling comes without the requirement of extra resources. We demonstrate the trapping and imaging of individual rubidium atoms and the in-plane assembly of defect-free single-atom arrays in several Talbot planes. We present interleaved lattices with dynamic position control and parallelized sub-lattice addressing of spin states.

Outstanding progress in atomic physics has paved the way for experiments which probe and exploit the laws of quantum mechanics at the single quantum level [1, 2]. A cornerstone are neutral atoms trapped by light, which constitute a versatile experimental platform where internal and external degrees of freedom can be coherently manipulated and interactions are dynamically tunable. This comprehensive control is the key element of forefront research in the extensive field of quantum technology, including quantum chemistry [3, 4], quantum interferometry [5], quantum metrology [6, 7], quantum information processing [8] and quantum simulation [9].

A natural focus are multi-site geometries created by optical lattices [10–13] and arrays of optical tweezers [14–26]. The former can serve as carriers for large numbers of isolated probes, thereby taintlessly boosting signal and sensitivity, as well as they can provide many-body systems with defined atom number per site and controllable tunnelling. Fostered by quantum gas microscopes with access to local observables, the top-down implementation of condensed matter models [11, 12] and the realization of optical clocks [27] has been demonstrated.

Flexible arrays of optical tweezers created by focused laser beams [14–26] decouple trap size and separation as well as array geometry from the constraint of interference, as imposed on optical lattices. Their inherently resolved trapping sites are adaptable to hold individual atoms [28] and can be composed from multiple colours of laser light [4, 16, 29]. Straightforward dynamic position control represents a fruitful tool which facilitates the coherent transport of quantum states [30–32] and the seminal assembly of defect free sub-arrays [17–19, 23, 25]. Thus, arrays of individually controlled microtraps lend themselves to the bottom-up engineering of quantum systems with configurable tunnel-coupling [33–35] and on-demand Rydberg interactions [8, 36, 37]. Pioneering implementations realized the fundamental building blocks of the Bose-Hubbard [33] and the Hubbard model [34], the formation of individual molecules [4] and small spin systems with Rydberg interactions ranging from dynam-

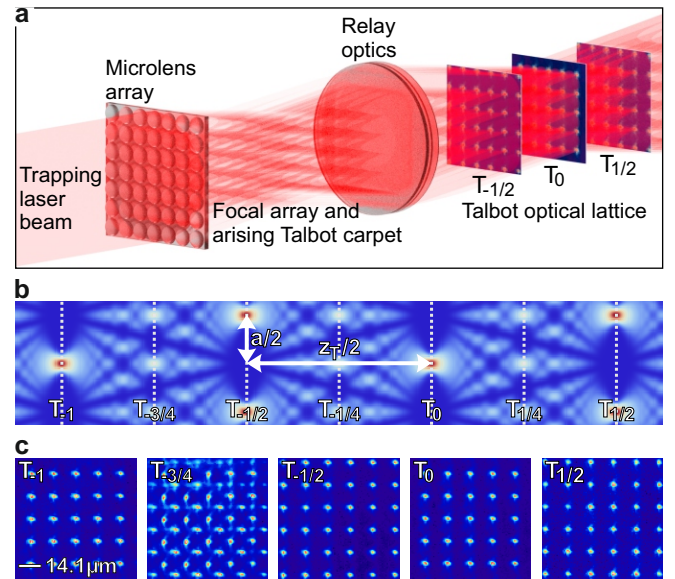


FIG. 1. 3D Talbot optical lattice generated by a microlens array. (a) Simplified schematic of the optical setup. The 2D periodic spot pattern of the focal plane of a microlens array gives rise to the formation of a 3D Talbot carpet. After demagnified reimaging, we obtain a multilayer stack of 2D periodic microtrap arrays formed from regular self-images of the generating focal plane (for clarity, only three planes are drawn). (b) 2D projection of the Talbot carpet created by an array of Gaussian beams with typical experimental parameters ($a = 14.1 \mu\text{m}$, $z_T = 497 \mu\text{m}$, $w_0 = 1.45 \mu\text{m}$). (c) Averaged fluorescence images of arrays of single atoms stored in integer and fractional Talbot planes (see text for details).

ically coupled to blockaded [17, 18, 37].

For future progress, scalability is pivotal. In this article, we respond to the evident need of a configurable large-scale implementation with a novel platform, as depicted in Fig. 1. We harness the Talbot effect [38, 39] to extend a microlens-array (MLA) generated 2D periodic configuration of single-atom microtraps to a stacked multilayer architecture in 3D. This Talbot optical lattice [40, 41] exhibits excellent scalability as it is created intrinsically

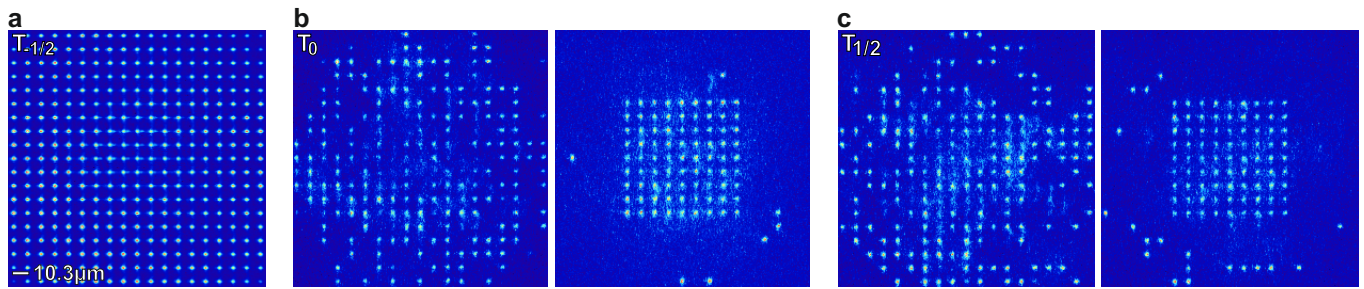


FIG. 2. Micro-optical realization of a Talbot optical lattice with hundreds of sites per principal plane and in-plane assembly of defect-free 9×9 clusters of individual atoms in different planes. (a) 19×19 site detail showing the averaged fluorescence at the resolved trapping positions of the plane $T_{-1/2}$. (b, c) Single-shot fluorescence images of individual atoms showing the initial atom distribution and successfully assembled atom clusters in the Talbot planes T_0 and $T_{1/2}$ (atom arrays are centered in the images). The assembly process involves multiple cycles of atom rearrangement and atom detection as detailed in Ref. [23].

and at no additional costs by the periodic microfabricated source element and the self-imaging Talbot effect. Figure 1(a) visualizes the experimental platform: The source element is a quadratic-grid MLA of 166×166 refractive lenslets with a pitch of $30.0(3) \mu\text{m}$. A subset of the lenslets is illuminated by the Gaussian laser beam with a beam waist of $200(2) \mu\text{m}$ at the position of the MLA and a wavelength of $\lambda = 798.6 \text{ nm}$. The 2D periodic spot pattern of the focal plane is the origin of a 3D Talbot carpet, which exhibits integer and fractional self-images (Talbot planes) of the generating pattern along the axis of beam propagation z . The separation of in lateral geometry and position identical self-images is given by the Talbot length $z_T = 2a^2/\lambda$, which is a function of the spatial pitch a of the generating pattern. Fractional self-images are found at fractional multiples of z_T and individual planes T are labeled according to their axial position normalized to z_T with the focal plane being the generating array. In our setup, the focal plane is reimaged and demagnified by the use of relay optics, which reduces the pitch and the associated Talbot length considerably. A noticeable modification due to reimaging is the appearance of negatively indexed Talbot planes which give rise to the resulting 3D Talbot optical lattice consisting of a series of Talbot planes along z centered at the reimaged focal plane T_0 . For the results presented in Fig. 1, we have generated a Talbot lattice with trap pitch of $a = 14.1(4) \mu\text{m}$ and trap waist of $w_0 = 1.45(10) \mu\text{m}$ at T_0 . The Talbot length evaluates to $z_T = 497(28) \mu\text{m}$. This corresponds to an axial separation of $z_T/2 = 248(14) \mu\text{m}$ of the principal planes $\dots, T_{-1}, T_{-1/2}, T_0, T_{1/2}, T_1, \dots$, which reproduce the in-plane structure of the focal plane. Figure 1(b) shows a 2D projection of the Talbot carpet in the region around the focal plane.

In our experiments, we prepare laser-cooled ^{85}Rb atoms in a magneto-optical trap and load them into the dipole trapping sites corresponding to the focal spots of the 3D Talbot lattice during a sequence of optical molasses (see [23] for further details). Typical trap depths are on the

order of $k_B \cdot 1 \text{ mK}$. For the detection of atoms in a specific 2D plane of the Talbot lattice, the imaging system is focused to the selected plane and the atoms in all other planes are removed with a resonant push-out laser beam. Figure 1(c) shows the averaged fluorescence images of individual atoms stored in the traps of the reimaged focal plane T_0 and of the Talbot planes T_{-1} , $T_{-3/4}$, and $T_{\pm 1/2}$. The trap positions are defined by the MLA and spatially resolved atom detection reveals the underlying periodic structure in the different planes. The principal planes hold 2D arrays of individual atoms in a quadratic grid with pitch a . In half-integer principal planes, the grid is shifted by $a/2$ in the x and y directions relative to T_0 . For the plane $T_{-3/4}$ the number of sites with observable atom fluorescence is increased, as expected for fractional Talbot planes. The trap pitch is reduced, but fluorescence is weaker and even vanishes for a subclass of sites at regular positions. We attribute this behaviour to a modulation of trap depths, which arises from interference effects of light transmitted by the lenslets and light transmitted through the interspaces of the MLA as well as from components of the light field produced by the spherical shape and limited aperture of the lenslets that are not included in a simple paraxial description underlying the calculation of the Talbot carpet [39, 42]. Each 2D Talbot plane can serve as an individual-atom quantum register with a readily scalable number of quantum systems. For the experimental implementation presented in Fig. 2, we use a quadratic-grid MLA with a pitch of $110.0(3) \mu\text{m}$, a diameter of $106(2) \mu\text{m}$, and a radius of curvature of $0.86(4) \text{ mm}$ for each lenslet. We utilize a trapping laser beam of wavelength 796.3 nm with a waist of $1923(21) \mu\text{m}$ at the position of the MLA which generates more than 400 optical microtraps in a principal plane. After demagnified reimaging, the trap pitch of the principal lattice planes is configured to $10.3(3) \mu\text{m}$ and the traps have a waist of $1.45(10) \mu\text{m}$. The Talbot length is $z_T = 267(15) \mu\text{m}$. Figure 2(a) gives an averaged fluorescence image of a 19×19 site detail of the plane $T_{-1/2}$. The preparation process based on light assisted collisions

results in a heavily sub-Poissonian distribution stemming from the effect of collisional blockade. On average, we prepare 191(17) atoms [23] and each site of the planar array is occupied by one atom at most. We observe a maximum probability to load an atom for the the central traps with a value of 0.6, which indicates the presence of two-body collisional events which cause only one of the participants (instead of both) to leave the trap. This channel allows for the near-deterministic preparation of single atoms [25].

The stochastic nature of the loading process leads to random atomic positions, whereas a broad range of applications pre-requires defect-free atomic arrays and the ability to mend atom loss during operation. This necessitates the incorporation of techniques for individual atom transport and deterministic target pattern assembly [17–19, 23, 25, 30, 31, 43]. For this purpose, we use a superposed moveable auxiliary laser beam, which acts as an optical tweezer. This technique is applicable to any Talbot plane in a straight-forward fashion. In our setup, the tweezer is aligned with the imaging system and therefore automatically focused to the selected plane. The principle of operation is detailed in [23], where it has been applied for the rearrangement of atoms in the reimaged focal plane T_0 . Starting from the initial atom distribution, a sequence of transport operations is performed in order to reach complete filling of the target structure and the resulting occupancy is analyzed. The detection of residual defects triggers another rearrangement cycle, which significantly enhances success rates and achievable structure sizes. In the work presented here, we define a 9×9 atomic cluster as target structure and the reservoir grid consists of 19×19 sites. Figures 2 (b,c) show in-situ fluorescence of the atomic pattern before and after successful assembly in the plane T_0 and $T_{1/2}$. The typical success rate is 12 % [23].

While the Talbot optical lattice produces a static 3D regular geometry with equidistant in-plane separation of atoms, advanced atom-optical experiments often build on elaborate arrangements, which incorporate parallelized transport [31], enable multi-species trapping [4, 36], can be configured to implement atomic subgroups and ancilla atoms [8, 44] and are adaptable to inhomogeneous interaction potentials [45]. In our architecture, we utilize interleaved Talbot optical lattices to extend the class of accessible geometries. These can be implemented by employing multiple MLAs as well as by the illumination of an individual MLA with multiple trapping laser beams. The latter approach results in axially superimposed lattice planes if the interleaved lattices are of near-identical wavelength. Lateral displacement of the trap arrays is achieved through a modification of incident angles on the MLA. While the displacement is a linear function of the MLAs focal length f_0 for the plane T_0 , for all other Talbot planes one has to consider the effective focal length which is enlarged by the absolute value of their axial

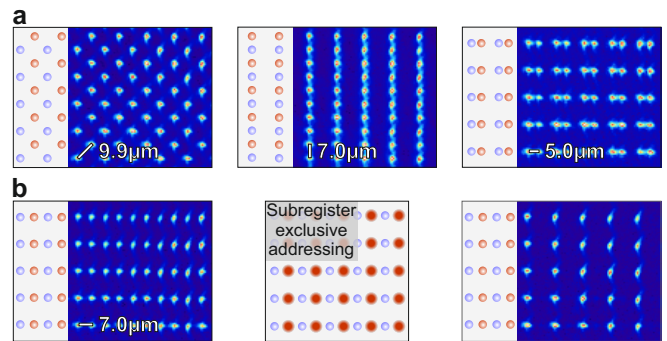


FIG. 3. Interleaved configuration of two Talbot lattices. All images show averaged fluorescence of the $T_{1/2}$ plane and the presented geometries are visualized by red and blue dots depicting the sites of the two lattices. (a) Single atom registers with tunable atomic separation. The separation of neighbouring traps is (from left to right): $9.9(3)\mu\text{m}$, $7.0(2)\mu\text{m}$, and $5.0(2)\mu\text{m}$. (b) Subregister exclusive addressing of stored atoms is used to convert a spin polarized register ($F = 2$, left) to a configuration of column-wise alternating spin states ($F = 2$ and $F = 3$, right). State-selective detection records fluorescence for atoms in $F = 2$ only.

separation from the focal plane before reimaging. Hence, working in a Talbot plane significantly reduces the required angle to reach a sufficient displacement as $f_0 < z_T$. This allows one to dynamically compose versatile quantum registers with flexible site separation from superimposed moveable subregisters which can be individually controlled. Each of the subregisters remains independently laser-addressable in a parallelized fashion through the MLA, which focuses the light onto the trapping sites and thereby amplifies the atom-light coupling. If the addressing beam is set to spatial overlap with the trapping light it is auto-aligned with the traps while the spacing of interleaved quantum registers can be arbitrarily set within the limits given by trap pitch and trap waist.

Figure 3 shows configurations created from two interleaved subregisters of the Talbot plane $T_{1/2}$ with fundamental pitch of $14.1(4)\mu\text{m}$. These are implemented by expanding the setup used in the first section with a second trapping laser beam having a waist of $202(2)\mu\text{m}$ and a frequency difference of 30.0 MHz to avoid interference effects. An enclosed angle of 12.3 mrad introduces an offset of half the trap pitch for the respective trap arrays. Figure 3 (a) (left) shows a uniform arrangement that reduces the pitch by a factor of $\sqrt{2}$ and forms a super-register with $9.9(3)\mu\text{m}$ trap separation, with each site of a respective subregister being equidistant to four sites of the other one. A multitude of atom-chains with $7.0(2)\mu\text{m}$ distance for the atoms within each column is created in Fig. 3 (a) (middle). Furthermore, the trap positions can be tuned to favour pairs of atoms as demonstrated with a separation of $5.0(2)\mu\text{m}$ for neighbouring atoms in Fig. 3 (a) (right). In the current implementation, traps stay independent for a minimum separation

of 3 μm which is consistent with the trap waist.

In the experiments of Fig. 3(b) we demonstrate subregister-wise parallelized laser-addressing with the transfer of the spin state of single atoms stored in subregisters with a spacing of 7.0(2) μm . First, all atoms in the complete set of traps are initialized to the $F = 2$ state of the ^{85}Rb ground state hyperfine manifold and state-selectively detected afterwards by removing the population of the $F = 3$ state prior to detection (left). The results displayed on the right account for a modified experimental sequence where laser addressing transfers the atoms to the $F = 3$ state in a subregister exclusive fashion, resulting in vanishing fluorescence at the addressed sites. The addressing beam at 795 nm is resonant to the transition $|5S_{1/2}, F = 2\rangle \leftrightarrow |5P_{1/2}, F = 3\rangle$ and is brought to spatial overlap with one of the trapping laser beams by using the same optical fiber. For the center trap, the occupation probability after initial state preparation is 0.47(2) and 0.01(1) after the subregister-exclusive state transfer. For the unaddressed subarray, we observe a reduction on the order of 2 %, which we contribute to chromatic aberrations.

A microlens-generated Talbot optical lattice allows for the creation of multi-site 3D trap arrays with customizable structure sizes in the micrometer regime. With the presented work, focused beam microtrap arrays enter a regime which has formerly been accessible only by phase-sensitive standing wave configurations, yet they retain the simplicity and robustness of the optical setup as well as their inherent features of coherent quantum state transport [31] and single-site addressability [46]. The straight-forward assembly of defect-free atomic arrays facilitates bottom-up engineering of quantum systems in microlens generated 2D and 3D trap arrays. In addition, atomic separations can be dynamically adapted in 3D using interleaved configurations, while subregister exclusive addressability extends techniques for the initialization and read out of quantum states and allows for the parallelization of operations. The implemented Talbot registers provide hundreds of single-addressable atoms at present with separations well within the limits for coherent Rydberg-mediated interactions with direct implications for neutral atom quantum information processing and quantum simulation architectures [8, 9, 36, 44, 47].

We acknowledge financial support from the Deutsche Forschungsgemeinschaft (DFG) through Grant No. BI 647/6-1 within the Priority Program SPP 1929 (GiRyd). We thank the *labscrip suite* community and J. Werkmann for support in implementing state-of-the-art control software for our experiments. We thank T. Preuschoff, L. Kohfahl, M.R. Sturm and R. Walser for insightful discussions.

-
- * malte.schlosser@physik.tu-darmstadt.de
 † gerhard.birkkl@physik.tu-darmstadt.de; www.iap.tu-darmstadt.de/apq
- [1] S. Haroche, Rev. Mod. Phys. **85**, 1083 (2013).
 - [2] D. J. Wineland, Rev. Mod. Phys. **85**, 1103 (2013).
 - [3] G. Qummer and P. S. Julienne, Chemical Reviews **112**, 4949 (2012).
 - [4] L. R. Liu, J. D. Hood, Y. Yu, J. T. Zhang, N. R. Hutzler, T. Rosenband, and K.-K. Ni, Science **360**, 900 (2018).
 - [5] A. D. Cronin, J. Schmiedmayer, and D. E. Pritchard, Rev. Mod. Phys. **81**, 1051 (2009).
 - [6] A. D. Ludlow, M. M. Boyd, J. Ye, E. Peik, and P. O. Schmidt, Rev. Mod. Phys. **87**, 637 (2015).
 - [7] C. L. Degen, F. Reinhard, and P. Cappellaro, Rev. Mod. Phys. **89**, 035002 (2017).
 - [8] M. Saffman, T. G. Walker, and K. Mølmer, Rev. Mod. Phys. **82**, 2313 (2010).
 - [9] I. M. Georgescu, S. Ashhab, and F. Nori, Rev. Mod. Phys. **86**, 153 (2014).
 - [10] I. Bloch, J. Dalibard, and S. Nascimbene, Nat Phys **8**, 267 (2012).
 - [11] C. Gross and I. Bloch, Science **357**, 995 (2017).
 - [12] P. Schauss, Quantum Science and Technology **3**, 023001 (2018).
 - [13] A. Kumar, T.-Y. Wu, F. Giraldo, and D. S. Weiss, Nature **561**, 83 (2018).
 - [14] R. Dumke, M. Volk, T. Mütter, F. B. J. Buchkremer, G. Birkel, and W. Ertmer, Phys. Rev. Lett. **89**, 097903 (2002).
 - [15] M. Schlosser, S. Tichelmann, J. Kruse, and G. Birkel, Quantum Information Processing **10**, 907 (2011).
 - [16] M. J. Piotrowicz, M. Lichtman, K. Maller, G. Li, S. Zhang, L. Isenhower, and M. Saffman, Phys. Rev. A **88**, 013420 (2013).
 - [17] H. Bernien, S. Schwartz, A. Keesling, H. Levine, A. Omran, H. Pichler, S. Choi, A. S. Zibrov, M. Endres, M. Greiner, *et al.*, Nature **551**, 579 (2017).
 - [18] H. Kim, Y. Park, K. Kim, H.-S. Sim, and J. Ahn, Phys. Rev. Lett. **120**, 180502 (2018).
 - [19] D. Barredo, V. Lienhard, S. De Léséleuc, T. Lahaye, and A. Browaeys, Nature **561**, 79 (2018).
 - [20] C. Sheng, X. He, P. Xu, R. Guo, K. Wang, Z. Xiong, M. Liu, J. Wang, and M. Zhan, Phys. Rev. Lett. **121**, 240501 (2018).
 - [21] M. A. Norcia, A. W. Young, and A. M. Kaufman, Phys. Rev. X **8**, 041054 (2018).
 - [22] A. Cooper, J. P. Covey, I. S. Madjarov, S. G. Porsev, M. S. Safronova, and M. Endres, Phys. Rev. X **8**, 041055 (2018).
 - [23] D. Ohl de Mello, D. Schäffner, J. Werkmann, T. Preuschoff, L. Kohfahl, M. Schlosser, and G. Birkel, arXiv preprint arXiv:1902.00284 (2019).
 - [24] S. Saskin, J. T. Wilson, B. Grinkemeyer, and J. D. Thompson, Phys. Rev. Lett. **122**, 143002 (2019).
 - [25] M. O. Brown, T. Thiele, C. Kiehl, T.-W. Hsu, and C. A. Regal, Phys. Rev. X **9**, 011057 (2019).
 - [26] L. Anderegg, L. W. Cheuk, Y. Bao, S. Burchesky, W. Ketterle, K.-K. Ni, and J. M. Doyle, arXiv preprint arXiv:1902.00497 (2019).
 - [27] G. E. Marti, R. B. Hutson, A. Goban, S. L. Campbell, N. Poli, and J. Ye, Phys. Rev. Lett. **120**, 103201 (2018).

- [28] N. Schlosser, G. Reymond, I. Protsenko, and P. Grangier, *Nature* **411**, 1024 (2001).
- [29] M. Schlosser, J. Kruse, and G. Birkl, arXiv preprint arXiv:1902.00370 (2019).
- [30] J. Beugnon, C. Tuchendler, H. Marion, A. Gaëtan, Y. Miroshnychenko, Y. R. Sortais, A. M. Lance, M. P. Jones, G. Messin, A. Browaeys, *et al.*, *Nature Physics* **3**, 696 (2007).
- [31] A. Lengwenus, J. Kruse, M. Schlosser, S. Tichelmann, and G. Birkl, *Phys. Rev. Lett.* **105**, 170502 (2010).
- [32] A. Kaufman, B. Lester, M. Foss-Feig, M. Wall, A. Rey, and C. Regal, *Nature* **527**, 208 (2015).
- [33] A. M. Kaufman, B. J. Lester, C. M. Reynolds, M. L. Wall, M. Foss-Feig, K. R. A. Hazzard, A. M. Rey, and C. A. Regal, *Science* **345**, 306 (2014).
- [34] S. Murmann, A. Bergschneider, V. M. Klinkhamer, G. Zürn, T. Lompe, and S. Jochim, *Phys. Rev. Lett.* **114**, 080402 (2015).
- [35] M. R. Sturm, M. Schlosser, R. Walser, and G. Birkl, *Phys. Rev. A* **95**, 063625 (2017).
- [36] M. Saffman, *Journal of Physics B: Atomic, Molecular and Optical Physics* **49**, 202001 (2016).
- [37] A. Browaeys, D. Barredo, and T. Lahaye, *Journal of Physics B: Atomic, Molecular and Optical Physics* **49**, 152001 (2016).
- [38] J. Wen, Y. Zhang, and M. Xiao, *Adv. Opt. Photon.* **5**, 83 (2013).
- [39] B. Besold and N. Lindlein, *Optical Engineering* **36**, 1099 (1997).
- [40] C. Mennerat-Robilliard, D. Boiron, J. M. Fournier, A. Aradian, P. Horak, and G. Grynberg, *EPL (Europhysics Letters)* **44**, 442 (1998).
- [41] Y. B. Ovchinnikov, *Phys. Rev. A* **73**, 033404 (2006).
- [42] H. Kim, W. Lee, H. Lee, and J. Ahn, *Phys. Rev. A* **91**, 033817 (2015).
- [43] M. Schlosser, J. Kruse, C. Gierl, S. Teichmann, S. Tichelmann, and G. Birkl, *New Journal of Physics* **14**, 123034 (2012).
- [44] H. Weimer, M. Muller, I. Lesanovsky, P. Zoller, and H. P. Büchler, *Nat Phys* **6**, 382 (2010).
- [45] S. de Léséleuc, V. Lienhard, P. Scholl, D. Barredo, S. Weber, N. Lang, H. P. Büchler, T. Lahaye, and A. Browaeys, arXiv preprint arXiv:1810.13286 (2018).
- [46] J. Kruse, C. Gierl, M. Schlosser, and G. Birkl, *Phys. Rev. A* **81**, 060308 (2010).
- [47] A. W. Glaetzle, R. M. van Bijnen, P. Zoller, and W. Lechner, *Nature Communications* **8**, 15813 (2017).